5937R

Bridgmanite-like crystal structure in the novel Ti-rich phase synthesized at transition zone condition

LUCA BINDI[1,2*], EKATERINA SIROTKINA[3,4], ANDREY V. BOBROV[3,4], MICHAEL J. WALTER[5], DMITRY PUSHCHAROVSKY[3], TETSUO IRIFUNE[6,7]

[1] Dipartimento di Scienze della Terra, Università di Firenze, Via La Pira 4, I-50121 Firenze, Italy
[2] CNR - Istituto di Geoscienze e Georisorse, sezione di Firenze, Via La Pira 4, I-50121 Firenze, Italy
[3] Geological Faculty, Moscow State University, Leninskie Gory, 119234, Moscow, Russia
[4] Vernadsky Institute of Geochemistry and Analytical Chemistry of Russian Academy of Sciences, 119991Moscow, Russia
[5] School of Earth Sciences, University of Bristol, Bristol BS8 1RJ, UK
[6] Geodynamics Research Center, Ehime University, Matsuyama 790-8577, Japan
[7] Earth-Life Science Institute, Tokyo Institute of Technology, Tokyo 152-8550, Japan

ABSTRACT

A new Ti-bearing bridgmanite-like phase with a three-fold commensurate superstructure of the ideal $MgSiO_3$-perovskite structure was observed in a $[Mg_{5/6}Al_{1/6}][Si_{1/2}Ti_{1/3}Al_{1/6}]O_3$ crystal synthesized in the model system $Mg_3Al_2Si_3O_{12}$–$MgTiO_3$ at 20 GPa and 1600 °C. The compound was found to be orthorhombic, space group $Pnma$, with lattice parameters $a = 14.767(3)$, $b = 6.958(1)$, $c = 4.812(1)$ Å, $V = 494.4(2)$ Å^3, which represents a $3\mathbf{a} \times \mathbf{b} \times \mathbf{c}$ superstructure of the typical $Pnma$ perovskite structure. The structure was refined to $R = 0.024$ using 846 independent reflections. The superstructure mainly arises from the ordering of titanium in one of the octahedral positions. Crystal-chemical details of the different polyhedra in the superstructure are discussed in comparison to pure $MgSiO_3$. This is the first documented superstructure of a bridgmanite phase, and Ti-rich bridgmanite in the lower mantle arising from local Ti-enrichments may exhibit different physical properties and elemental partitioning behavior from Ti-poor, peridotitic bridgmanite. The study also shows that large amounts of Ti can stabilize bridgmanite-like compounds at considerably lower pressure than lower mantle conditions.

KEYWORDS: bridgmanite, titanium, lower mantle, crystal structure, microprobe analysis, synthesis

INTRODUCTION

Normal mantle peridotite contains ~0.2 wt% TiO_2 (e.g. McDonough and Sun 1995). However, Ti-rich lithologies may occur in the mantle as a result of oceanic crust subduction.

Mid-ocean ridge basalt has about 1.5 wt% TiO_2, whereas ocean island basalt may contain about twice that amount (e.g. Wilson 1989). Experiments show that the solubility of titanium in subduction zone fluids is very low (e.g. Audetat and Keppler 2005; Tropper and Manning 2005), so that during slab dehydration TiO_2 should be retained in subducting crust and transported eventually into the lower mantle.

According to experimental data (e.g. Walter et al. 2004; Liebske et al. 2005), bridgmanite in primitive mantle peridotite will contain about 0.2–0.3 wt% TiO_2. This estimate is consistent with inclusions in diamonds that have been interpreted to represent samples of peridotitic bridgmanite (e.g. Harte 2010). However, some composite inclusions in diamonds have been interpreted as the products of retrograde unmixing of former bridgmanite formed in subducted oceanic crust, and these have much higher TiO_2 contents ranging between about 4 and 7 wt% TiO_2 (Walter et al. 2011; Thomson et al. 2014; Zedgenizov et al. 2015).

Low-degree melts formed either in subducted crust or in the mantle as a consequence of volatile enrichment (e.g. CO_2 or water) are also expected to contain several weight percent levels of TiO_2 (e.g. Thomson et al. 2016), and reaction of these melts with surrounding mantle may produce local enrichments in TiO_2. For example, inclusions in diamonds interpreted to represent former Ca-rich perovskite can contain more than 50 mol% of $CaTiO_3$ component (Brenker et al. 2005; Walter et al. 2008) and these have been interpreted to represent reaction between low-degree melts and mantle peridotite in the transition zone (Walter et al. 2008; Armstrong et al. 2012; Thomson et al. 2016). A similar process in the lower mantle would also be expected to leave TiO_2 enriched domains, with implications for the crystal chemistry, thermo-elastic properties and structure of bridgmanite.

In order to understand the potential role of Ti-rich bridgmanite in the deep mantle, we must first quantify the affect of Ti incorporation on the bridgmanite structure. To this end, we performed experiments on a Ti-rich $MgSiO_3$-bridgmanite composition in the model system pyrope (Prp–$Mg_3Al_2Si_3O_{12}$) – geikielite (Gkl–$MgTiO_3$) at 20 GPa and 1600 °C. Here we present the results of a structural study based on X-ray diffraction data from a bridgmanite-like single crystal with the highest Ti content ever reported. We find that the ordering of titanium in the structure is responsible for the occurrence of a three-fold superstructure.

EXPERIMENTAL

Synthesis

The starting material was made by mixing pure oxides of MgO, SiO_2, Al_2O_3 and TiO_2 in stoichiometric proportions to make the composition pyrope (Prp–$Mg_3Al_2Si_3O_{12}$) – geikielite (Gkl–$MgTiO_3$) $Prp_{30}Gkl_{70}$ (mol.%). The experiment that produced run product 1608-70 was

2

75   carried out at P = 20 GPa and T = 1600 °C using a 1000-t Kawai-type multi-anvil apparatus

76   installed at the Ehime University (Matsuyama, Japan). Samples were compressed by eight

77   cubic tungsten carbide anvils with 4-mm truncation edge lengths, and using pyrophyllite as a

78   gasketing material. High temperature was achieved using a cylindrical $LaCrO_3$ heater, and

79   temperature was measured with a $W_{97}Re_3$–$W_{75}Re_{25}$ thermocouple. The sample was loaded

80   into a platinum capsule and was isolated from the heater by an MgO insulator (Sirotkina et al.

81   2015). The approximate sample volume after the experiment was 1.0 mm^3. Sample pressure

82   was calibrated at room temperature using the semiconductor–metal transitions of Bi, ZnS and

83   GaAs (Irifune et al. 2004). The effect of temperature on pressure was further corrected using

84   the α–β and β–γ phase transitions of olivine (Katsura and Ito 1989; Yamada et al. 2004). Ti-

85   bearing bridgmanite-like phase was the modally dominant phase in the run product, and was

86   accompanied by a minor amount of periclase and rutile (Fig. 1), in keeping with the reaction:

87   $7MgTiO_3$ (giekelite) + $3Mg_3Al_2Si_3O_{12}$ (pyrope) → $3Mg_5Al_2Ti_2Si_3O_{18}$ (Ti-Brd) + TiO_2 (rutile)

88   + MgO (periclase).

Data collection and crystal-structure solution and refinement

90   A small crystal (38 × 52 × 55 μm), hand-picked under a reflected light microscope from

91   the run product 1608-70 (Fig. 1), was preliminarily examined with a Bruker-Enraf MACH3

92   single-crystal diffractometer using graphite-monochromatized Mo$K\alpha$ radiation. The measured

93   orthorhombic cell parameters are: a_s = 14.767(3), b_s = 6.958(1), c_s = 4.812(1) Å, which

94   represents a $3\mathbf{a}_b × \mathbf{b}_b × \mathbf{c}_b$ superstructure of the typical $Pnma$ perovskite structure with a_b =

95   4.9, b_b = 6.9, c_b = 4.8 Å (the subscripts "s" and "b" mean superstructure and basic structure,

96   respectively). Next, data were collected with an Oxford Diffraction Xcalibur 3 diffractometer

97   (X-ray Mo$K\alpha$ radiation, λ = 0.71073 Å) fitted with a Sapphire 2 CCD detector (with 130 s

98   exposure time per frame). Intensity integration and standard Lorentz-polarization corrections

99   were done with the $CrysAlis$ RED (Oxford Diffraction 2006) software package. The program

100 ABSPACK of the $CrysAlis$ RED package (Oxford Diffraction 2006) was used for the

101 absorption correction. The R_{int} (Laue group mmm) decreased from 0.076 to 0.032 after the

102 absorption correction. A careful inspection of the frames (and of the reconstructed precession

103 photographs) collected in the present study did not reveal any reflection streaks and/or

104 structural disorder. The reflections were quite sharp and not 'structured'.

105 Taking into account (i) the results obtained by the analysis of reflection conditions ($0kl$:

106 $k+l = 2n$, $hk0$: $h = 2n$; $h00$: $h = 2n$, $0k0$: $k = 2n$; $00l$: $l = 2n$), (ii) the distribution of $|E|$ values

107 that strongly indicated the presence of an inversion centre ($|E^2 - 1|$ = 0.990), and (iii) the fact

108 that the maximal $klassengleiche$ subgroup of the space group $Pnma$ (with an enlarged three-

109 fold unit cell) is still $Pnma$, attempts to solve the crystal structure were made in this space

3

group. The Mg atom site of the *Pnma* bridgmanite structure (Wyckoff position 4*c*) splits into three new 4*c* positions (MgA, MgB, and MgC), whereas the Si atom site (Wyckoff position 4*b*) splits into two 4*b* and 8*d* positions. The full-matrix least-squares program SHELXL-97 (Sheldrick 2008), working on F^2, was used for the refinement of the structure. Site-scattering values were refined at the Mg and octahedral sites using scattering curves for neutral species (Ibers and Hamilton 1974) as follows: Mg vs. [] and Ti vs. []. The O sites (refined as O vs. []) were found fully occupied, and the occupancy factors were then fixed to 1.00. Two Mg sites (i.e., MgA and MgB) showed a site scattering of 12 electrons and were thought to be fully occupied by Mg and fixed accordingly (in agreement with the observed bond distances – see below), whereas the MgC site showed a mean electron number of 12.4, thus indicating the presence of a small amount of a heavier element than Mg. From the analysis of the site geometry, we attributed a $Mg_{0.50}Al_{0.50}$ population (electron number of 12.5) to this site. One of the octahedral sites (4*b* site) was found fully occupied by Ti, whereas the second octahedral site showed a mean electron number of 13.9, thus indicating the presence of a small amount of a lighter element than Si. Taking into account the chemical composition of the crystal, the crystal-chemical details and the already site-assigned elements, we attribute a $Si_{0.75}Al_{0.25}$ population (electron number of 13.8) to this site. The refinement of the site occupancy with the restrictions described above, produced an overall stoichiometry of $Mg_8(Mg_2Al_2)[Ti_4(Si_6Al_2)]O_{36}$, which, with $Z = 4$ and grouping together the same atomic species, can be written as $(Mg_{2.5}Al_{0.5})[Ti(Si_{1.5}Al_{0.5})]O_9$. If we write the formula on the basis of three oxygen atoms, it is $[Mg_{0.83}Al_{0.17}][Si_{0.50}Ti_{0.33}Al_{0.17}]O_3$, or $[Mg_{5/6}Al_{1/6}][Si_{1/2}Ti_{1/3}Al_{1/6}]O_3$.

Successive cycles were run introducing anisotropic temperature factors for all the atoms leading to $R1 = 0.024$ for 846 observed reflections $[F_o > 4\sigma(F_o)]$ and $R1 = 0.029$ for all 2312 independent reflections and 80 parameters. Bond distances are reported in Table 1, whereas fractional atomic coordinates, atomic displacement parameters and the list of the observed and calculated structure factors are in the CIF[1].

Chemical composition

A preliminary chemical analysis using energy dispersive spectrometry, performed on the same crystal fragment used for the structural study as well as on other fragments from the same run product, did not indicate the presence of elements ($Z > 9$) other than Ti, Al, Mg and Si. The chemical composition was then determined using wavelength dispersive analysis (WDS) by means of a Jeol JXA-8600 electron microprobe. We used 40 s as counting time. The matrix correction was performed with the Bence and Albee (1968) program as modified

---

[1] For a copy of CIF, document item ……., contact the Business Office of the Mineralogical Society of America.

143 by Albee and Ray (1970). The standards employed were forsterite (Mg, Si), synthetic Al_2SiO_5

144 (Al), and synthetic TiO_2 (Ti). The crystal used for the X-ray study was found to be

145 homogeneous within the analytical uncertainty. The average chemical composition (six

146 analyses on different spots) is (wt %): MgO 31.03(12); SiO_2 28.14(18); TiO_2 25.20(10);

147 Al_2O_3 15.80(11); total 100.17(18); corresponding, on the basis of 3 oxygen atoms, to

148 $[Mg_{0.824(8)}Si_{0.501(9)}Ti_{0.338(7)}Al_{0.332(8)}]O_3$.

149

RESULTS AND DISCUSSION

151 On the whole, the crystal structure of the Ti-rich bridgmanite-like phase (Fig. 2) is

152 topologically similar to that of $MgSiO_3$ bridgmanite. The three-fold commensurate

153 superstructure is mainly due to the ordering of titanium in one of the octahedral sites. The

154 mean bond distances observed for the two pure Mg-polyhedra (2.219 and 2.222 Å, for MgA

155 and MgB, respectively) are very close to that observed in pure $MgSiO_3$ (2.205 Å; Dobson and

156 Jacobsen 2004). On the contrary, the shorter mean bond distance observed for MgC (2.152 Å)

157 is in agreement with the presence of Al replacing Mg. The octahedral site fully occupied by

158 Ti shows a mean bond distance of 1.924 Å, which is slightly shorter than the <Ti-O> distance

159 observed in rutile (1.958 Å; Swope et al. 1995) and in $CaTiO_3$ perovskite (1.953 Å;

160 Yamanaka et al. 2002). The $(Si_{0.75}Al_{0.25})$ octahedron exhibits a mean bond distance of 1.766

161 Å, which is slightly larger than that observed in stishovite (1.757 Å; Hill et al. 1983) in

162 agreement with the presence of Al replacing Si. The proposed cation distribution is in

163 agreement with the bond valence analysis carried out using the parameters reported by Brese

164 and O'Keeffe (1991), i.e. MgA = 2.19, MgB = 2.06, MgC = 2.47, Ti = 4.29, Si = 4.05, O1 =

165 2.09, O2 = 2.28, O3 = 1.95, O4 = 2.14, O5 = 2.19, and O6 = 2.15 *v.u.*.

166 The unit-cell of the Ti-rich bridgmanite-like phase is: a = 14.767(3), b = 6.958(1), c =

167 4.812(1) Å. If we consider $a/3$ (in order to easily compare the average unit cell of the

168 superstructure and the normal bridgmanite structure), we get the value of 4.922 Å. Then, by

169 converting the *Pnma* setting in the conventionally reported *Pbnm* space group of bridgmanite,

170 we get (for Ti-Brd): a = 4.812, b = 4.922, c = 6.958 Å, V = 164.8 Å^3. Several interesting

171 crystal-chemical parameters can be calculated, as the tilt among octahedra. The simplest

172 method of estimating tilt angles between octahedra in *Pbnm* perovskites is from the unit-cell

173 parameters. Provided the octahedra remain regular, the tilt angle can be related to a single

174 rotation about the [111] pseudocubic axis, designated as Φ, and given by the relation: $\Phi = \cos^{-1}(\text{sqrt2 } a^2/bc)$] (e.g. O'Keeffe et al. 1979). In the case of Ti-Brd, neglecting the fact that we

176 are now considering an average *Pbnm* structure and not ideal polyhedra, the value is 17.02°. If

177 we plot our datum in the diagram proposed by Sinmyo et al. (2014) and consider a *x*-value

(Fe+Al) = 0.34 a.p.f.u., the Ti-bridgmanite-like phase (filled red circle in Fig. 3) falls close to the trend of $(Mg,Fe)SiO_3$ perovskites. However, in this diagram Ti is not considered. If we consider the influence of Ti similar to that of trivalent cations in perovskites, the x-value in Figure 3 is 0.67 a.p.f.u and the behavior would be intermediate (empty red circle in Fig. 3) between those observed for the series $(Mg,Fe)SiO_3$ and those in $(Mg,Fe)(Si,Al)O_3$ perovskites. Even more interesting, if we consider the overall mean of the volumes of the MgO_{12} polyhedra [MgA 37.40 Å^3; MgB 35.63 Å^3; MgC (which hosts Al) 33.31 Å^3], 35.45 Å^3, and the overall mean of the two octahedral-site volumes [one hosting Ti (9.36 Å^3) and one hosting $Si_{0.75}Al_{0.25}$ (7.20 Å^3)], taking into account the different multiplicity of the two sites, we get 7.92 Å^3. The ratio of the two volumes, V_X/V_Y, is 4.476. Then, if we calculate the overall polyhedral tilting Φ defined as $1 - \cos2\theta m\cos\theta z$ (Thomas 1996), we get 0.0873, perfectly in line with the predicted trend. We note that V_X/V_Y = 4.477 and Φ = 0.0872 are nearly identical to those for pure $MgSiO_3$ (Dobson and Jacobsen 2004). However, this is not surprising, considering that in Ti-Brd there is a smaller $<V_X>$ compared to $MgSiO_3$ because of the presence of Al replacing Mg at the MgC site. However, the MgA and the MgB sites are more expanded with respect to the Mg site in $MgSiO_3$, thus resulting in a higher average value (i.e., $<V_X>$ = 35.45 Å^3 compared to 34.38 Å^3 in $MgSiO_3$). Furthermore, in Ti-Brd we have one octahedral site fully occupied by Ti^{4+}, which is larger than Al^{3+}. This gives rise to an overall $<V_Y>$ of 7.92 Å^3, which is slightly higher than that observed for the octahedral Si in $MgSiO_3$ (7.68 Å^3). As a consequence, the ratio between the X and Y volumes in Ti-Brd and pure $MgSiO_3$ is almost identical. It is very likely that the cation ordering responsible for the occurrence of the superstructure is thermodynamically favored (with respect to a disordered structure) to reduce lattice strains.

The (Al,Ti)–for–(Mg,Si) substitution also induces a strong distortion of the octahedral site quantifiable with an increase of the octahedral angle variance σ^2 (Robinson et al. 1971) from 1.56 in pure $MgSiO_3$ (Dobson and Jacobsen 2004) to an average weighted value of 37.02 in Ti-Brd ($\sigma^2_{Ti\ site}$ = 29.13 and $\sigma^2_{(Si,Al)\ site}$ = 40.97). A slight increase of distortion with respect to pure $MgSiO_3$ was also noticed in Al-bearing (Kojitani et al. 2007) and Cr-bearing (Bindi et al. 2014) bridgmanite.

IMPLICATIONS

The new Ti-bridgmanite-like phase was synthesized at a transition zone pressure (20 GPa), even though it has a very similar crystal structure to the most abundant mineral in the lower mantle, $MgSiO_3$ bridgmanite, which becomes stable at about 24 GPa (Tschauner et al. 2014). This suggests that unlike Al (Kubo and Akaogi 2000), Ti-incorporation stabilizes the

bridgmanite-type structure to lower pressure, as is also the case for Ti-rich calcium perovskite (Kubo et al. 1997). Armstrong et al. (2012) investigated phase relations along the $MgSiO_3$-$MgTiO_3$ join and their data at ~25 GPa indicate a relatively modest solubility of $MgTiO_3$-component into bridgmanite (~10 mol%). Their results also indicate immiscibility with an $MgTiO_3$-rich phase. These authors observed an increase in $MgTiO_3$ solubility with pressure in bridgmanite, and their phase relations suggest closing of a miscibility gap between $MgSiO_3$-rich and $MgTiO_3$-rich phases by ~ 50 GPa. The new bridgmanite-like phase found here may represent the Ti-rich conjugate phase in this system.

It is not yet clear at what Ti-content this new Ti-bridgmanite-like phase stabilizes, or its minimum pressure stability, so it is difficult to assess its potential role in the mantle. The bulk Ti content is too low in mantle peridotite (~0.2%), and likely too low in subducted oceanic crust (~ 1–3%), to directly stabilize this new phase. However, inclusions in some superdeep natural diamonds provide evidence for Ti-rich domains at transition zone depths that are likely related to metasomatism by low-degree melts (e.g. Thomson et al. 2016). The new Ti-bridgmanite-like phase is potentially stable in such Ti-rich environments, where it could have important geochemical effects or act as a tracer for metasomatic processes. However, this phase has yet to be reported in natural diamonds. Further work is needed to determine the pressure-temperature-composition stability of this phase, and to determine its thermo-physical and chemical properties.

REFERENCES CITED

Albee, A.L., and Ray, L. (1970) Correction factors for electron probe analysis of silicate, oxides, carbonates, phosphates, and sulfates. Analytical Chemistry, 48, 1408-1414.

Andrault, D., Bolfan-Casanova, N., and Guignot, N. (2001) Equation of state of lower mantle (Al,Fe)-$MgSiO_3$ perovskite. Earth and Planetary Science Letters, 193, 501-508.

Armstrong, L.S., Walter, M.J., Tuff, J.R., Lord, O.T., Lennie, A.R., Kleppe, A.K., and Clarke, S.M. (2012) Perovskite phase relations in the system CaO-MgO-TiO_2-SiO_2 and implications for deep mantle lithologies. Journal of Petrology, 53, 611-635.

Audetat, A., and Keppler, H. (2005) Solubility of rutile in subduction zone fluids, as determined by experiments in the hydrothermal diamond anvil cell. Earth and Planetary Science Letters, 232, 393-402.

Bence, A.E., and Albee, A.L. (1968) Empirical correction factors for the electron microanalysis of silicate and oxides. Journal of Geology, 76, 382-403.

Bindi, L., Sirotkina, E.A., Bobrov, A.V., and Irifune, T. (2014) Chromium solubility in perovskite at high pressure: The structure of $(Mg_{1-x}Cr_x)(Si_{1-x}Cr_x)O_3$ (with $x = 0.07$) synthesized at 23 GPa and 1600 °C. American Mineralogist, 99, 866-869.

Boffa Ballaran, T., Kurnosov, A., Glazyrin, K., Frost, D.J., Merlini, M., Hanfland, M., and Caracas, R. (2012) Effect of chemistry on the compressibility of silicate perovskite in the lower mantle. Earth and Planetary Science Letters, 333-334, 181-190.

Bolfan-Casanova, N. (2000) The distribution of water in the Earth's mantle: an experimental and infrared spectroscopic study. University of Bayreuth, Dissertation.

Brenker F.E., Vincze L., Vekemans B., Nasdala L., Stachel T., Vollmer, C,. Kersten, M., Somogyif, A., Adams, F., Joswig, W., and Harris, J.W. (2005) Detection of a Ca-rich lithology in the Earth's deep (300 km) convecting mantle. Earth and Planetary Science Letters, 236, 579-587.

Brese, N.E., and O'Keeffe, M. (1991) Bond-valence parameters for solids. Acta Crystallographica, B47, 192-197.

Catalli, K., Shim, S.H., Dera, P., Prakapenka, V.B., Zhao, J., Sturhahn, W., Chow, P., Xiao, Y., Cynn, H., and Evans, W.J. (2011) Effects of the Fe^{3+} spin transition on the properties of aluminous perovskite. New insights for lower-mantle seismic heterogeneities. Earth and Planetary Science Letters, 310, 293-302.

Dobson, D.P., and Jacobsen, S.D. (2004) The flux growth of magnesium silicate perovskite single crystals. American Mineralogist, 89, 807-811.

Fei, Y., Wang, Y., and Finger, L.W. (1996) Maximum solubility of FeO in $(Mg,Fe)SiO_3$-perovskite as a function of temperature at 26 GPa: implication for FeO content in the lower mantle. Journal of Geophysical Research, 101, 11525-11530.

Fiquet, G., Andrault, D., Dewaele, A., Charpin, T., Kunz, M., and Hausermann, D. (1998) P–V–T equation of state of $MgSiO_3$ perovskite. Physics of the Earth and Planetary Interiors, 105, 21-31.

Harte, B. (2010) Diamond formation in the deep mantle: the record of mineral inclusions and their distribution in relation to mantle dehydration zones. Mineralogical Magazine, 74, 189-215.

Hill, R.J., Newton, M.D., and Gibbs, G.V. (1983) A crystal chemical study of stishovite. Journal of Solid State Chemistry, 47, 185-200.

Hummer, D.R., and Fei, Y. (2012) Synthesis and crystal chemistry of Fe^{3+}-bearing $(Mg, Fe^{3+})(Si, Fe^{3+})O_3$ perovskite. American Mineralogist, 97, 1915-1921.

Ibers, J.A., and Hamilton, W.C., Eds. (1974) *International Tables for X-ray Crystallography*, vol. IV, 366p. Kynock, Dordrecht, The Netherlands.

Irifune, T., Kurio, A., Sakamoto, S., Inoue, T., Sumiya. H., and Funakoshi, K. (2004) Formation of pure polycrystalline diamond by direct conversion of graphite at high pressure and high temperature. Physics of the Earth and Planetary Interiors, 143-144, 593-600.

Ito, E., and Yamada H. (1982) Stability relations of silicate spinels, ilmenites and perovskite. In: Akimoto S, Manghnani MH (eds) High pressure research in geophysics. Center for Publications, Tokyo, pp 405-419.

Jephcoat, A.P., Hriljac, J.A., McCammon, C.A., O'Neill, H.S.C., Rubie, D.C., and Finger L.W. (1999) High resolution synchrotron X-ray powder diffraction and Rietveld

structure refinement of two $(Mg_{0.95},Fe_{0.05})SiO_3$ perovskite samples synthesized under different oxygen fugacity conditions. American Mineralogist, 84, 214-220.

Katsura, T., and Ito, E. (1989) The system Mg_2SiO_4-Fe_2SiO_4 at high pressure and temperatures: precise determination of stabilities of olivine, modified spinel, and spinel. Journal of Geophysical Research, 94, 15663-15670.

Kojitani, H., Katsura, T., and Akaogi, M. (2007) Aluminum substitution mechanisms in perovskite-type $MgSiO_3$: an investigation by Rietveld analysis. Physics and Chemistry of Minerals, 34, 257-267.

Kubo, A., and Akaogi, M. (2000) Post-garnet transitions in the system $Mg_4Si_4O_{12}$ – $Mg_3Al_2Si_3O_{12}$ up to 28 GPa: phase relations of garnet, ilmenite and perovskite. Physics of the Earth and Planetary Interiors, 121, 85-102.

Kubo, A. Suzuki, T., and Akaogi, M. (1997) High pressure phase equilibria in the system $CaTiO_3$-$CaSiO_3$: stability of perovskite solid solutions. Physics and Chemistry of Minerals, 24, 488-494.

Kudoh, Y., Prewitt, C.T., Finger, L.W., Darovskikh, A., and Ito, E. (1990) Effect of iron on the crystal structure of (Mg, Fe)SiO3 perovskite. Geophysical Research Letters, 17, 1481-1484.

Liebske, C., Corgne, A., Frost, D.J., Rubie, D.C., and Wood, B.J. (2005) Compositional effects on element partitioning between Mg-silicate perovskite and silicate melts. Contributions to Mineralogy and Petrology, 149, 113-128.

Mao, H.K., Hemley, R.J., Fei, Y., Shu, J.F., Chen, L.C., Jephcoat, A.P., Wu, Y., Bassett, W.A. (1991) Effect of pressure, temperature and composition on lattice parameters and density of (Fe,Mg)SiO_3-perovskites to 30 GPa. Journal of Geophysical Research, 96, 8069-8079.

McCammon, C.A., Rubie, D.C., Ross, C.R. II, Seifert, F., and O'Neill, H.S.C. (1992) Mossbauer spectra of $^{57}Fe_{0.05}Mg_{0.95}SiO_3$ perovskite at 80 and 298 K. American Mineralogist, 77, 894-897.

McDonough, W.F., and Sun, S.-S. (1995) The compositoon of the Earth. Chemical Geology, 120, 223-253.

Nishio-Hamane, D., Nagai, T., Fujino, K., and Seto, Y., and Takafuji, N. (2005) Fe^{3+} and Al solubilities in $MgSiO_3$ perovskite: implication of the $Fe^{3+}AlO_3$ substitution in $MgSiO_3$ perovskite at the lower mantle condition. Geophysical Research Letters, 32, L16306.

Nishio-Hamane, D., Seto, Y., Fujino, K., and Nagai, T. (2008) Effect of $FeAlO_3$ incorporation into $MgSiO_3$ on the bulk modulus of perovskite. Physics of the Earth and Planetary Interiors, 166, 219-225.

O'Keeffe, M., Hyde, B.G., and Bovin, J.O. (1979) Contribution to the crystal chemistry of orthorhombic perovskite: $MgSiO_3$ and $NaMgF_3$. Physics and Chemistry of Minerals, 4, 299-305.

Oxford Diffraction (2006) *CrysAlis* RED (Version 1.171.31.2) and ABSPACK in *CrysAlis* RED. Oxford Diffraction Ltd, Abingdon, Oxfordshire, England.

Parise, J.B., Wang, Y., Yeganeh-Haeri, A., Cox, D.E., and Fei, Y. (1990) Crystal structure and thermal expansion of (Mg,Fe)SiO_3 perovskite. Geophysical Research Letters, 17, 2089-2092.

Robinson, K., Gibbs, G.V., and Ribbe, P.H. (1971) Quadratic elongation: a quantitative measure of distortion in coordination polyhedra. Science, 172, 567-570.

Saikia, A., Boffa Ballaran, T., and Frost, D.J. (2009) The effect of Fe and Al substitution on the compressibility of $MgSiO_3$-perovskite determined through single-crystal X-ray diffraction. Physics of the Earth and Planetary Interiors, 173, 153-161.

Sheldrick, G.M. (2008) A short history of SHELX. Acta Crystallographica, A64, 112-122.

9

Sinmyo, R., Bykova, E., McCammon, C., Kupenko, I., Potapkin, V., and Dubrovinsky L. (2014) Crystal chemistry of Fe^{3+}-bearing (Mg,Fe)SiO$_3$ perovskite: a single-crystal X-ray diffraction study. Physics and Chemistry of Minerals, 41, 409-417.

Sirotkina, E.A, Bobrov, A.V., Bindi, L., and Irifune, T. (2015) Phase relations and formation of chromium-rich phases in the system Mg$_4$Si$_4$O$_{12}$–Mg$_3$Cr$_2$Si$_3$O$_{12}$ at 10–24 GPa and 1,600 °C. Contributions to Mineralogy and Petrology, 169, 2, doi10.1007/s00410-014-1097-0.

Swope, R.J., Smyth, J.R., and Larson, A.C. (1995) H in rutile-type compounds: I. Single-crystal neutron and X-ray diffraction study of H in rutile. American Mineralogist, 80, 448-453.

Tange, Y., Takahashi, E., Nishihara, Y., Funakoshi, K., and Sata N. (2009) Phase relations in the system MgO–FeO–SiO$_2$ to 50 GPa and 2000 °C: an application of experimental techniques using multianvil apparatus with sintered diamond anvils. Journal of Geophysical Research, 114, B02214.

Thomas, N.W. (1996) The compositional dependence of octahedral tilting in orthorhombic and tetragonal perovskites. Acta Crystallographica, B52, 16-31.

Thomson, A.R., Kohn, S.C., Bulanova, G.P., Smith, C.B., Araujo, D., EIMF, and Walter, M.J. (2014) Origin of sub-lithospheric diamonds from the Juina-5 kimberlite (Brazil): constraints from carbon isotopes and inclusion compositions. Contributions to Mineralogy and Petrology, 168, 1081.

Thomson, A.R., Walter, M.J., Kohn, S.C., and Brooker, R.A. (2016) Slab melting as a barrier to deep carbon subduction. Nature, 529, 76-79.

Tropper, P., and Manning, C.E. (2005) Very low solubility of rutile in H$_2$O at high pressure and temperature, and its implications for Ti mobility in subduction zones. American Mineralogist, 90, 502-505.

Tschauner, O., Ma, C., Beckett, J.R., Prescher, C., Prakapenka, V., and Rossman, G.R. (2014) Discovery of bridgmanite, the most abundant mineral in Earth, in a shocked meteorite. Science, 346, 1100-1102.

Vanpeteghem, C.B., Angel, R.J., Ross, N.L., Jacobsen, S.D., Dobson, D.P., Litasov, K.D., and Ohtani, E. (2006) Al, Fe substitution in the MgSiO$_3$ perovskite structure: a single-crystal X-ray diffraction study. Physics of the Earth and Planetary Interiors, 155, 96-103.

Walter, M.J., Bulanova, G.P., Armstrong, L.S., Keshav, S., Blundy, J.D., Gudfinnsson, G., Lord, O.T., Lennie, A.R., Clark, S.M., Smith, C.B., and Gobbo, L. (2008) Primary carbonatite melt from deeply subducted oceanic crust. Nature, 454, 622-625.

Walter, M.J., Kohn, S.C., Araujo, D., Bulanova, G.P., Smith, C.B., Gaillou, E., Wang, J., Steele, A., and Shirey, S.B. (2011) Deep mantle cycling of oceanic crust: evidence from diamonds and their mineral inclusions. Science, 334, 54-57.

Walter, M.J., Kubo, A., Yoshino, T., Brodholt, J., Koga, K.T., and Ohishi, Y. (2004) Phase relations and equation-of-state of aluminous Mg–Silicate perovskite and implications for Earth's lower mantle. Earth and Planetary Science Letters, 222, 501-516.

Wang, Y., Weidner, D.J., Liebermann, R.C., and Zhao, Y. (1994) P–V–T equation of state of (Mg,Fe)SiO$_3$ perovskite: constraints on composition of the lower mantle. Physics of the Earth and Planetary Interiors, 83, 13-40.

Wilson, M. (1989) Igneous petrogenesis – A global tectonic approach. Dordrecht, Kluwer Academic Publishers, 466 p.

Yamada, A., Inoue, T., and Irifune, T. (2004) Melting of enstatite from 13 to 18 GPa under hydrous conditions. Physics of the Earth and Planetary Interiors, 147, 45-56.

Yamanaka, T., Hirai, M., and Komatsu, Y. (2002) Structure change of Ca$_{1-x}$Sr$_x$TiO$_3$ perovskite with composition and pressure. American Mineralogist, 87, 1183-1189.

Zedgenizov, D.A., Shatsky, V.S., Panin, A.V. , Evtushenko, O.V., Ragozin, A.L., and Kagi, H. (2015) Evidence for phase transitions in mineral inclusions in superdeep diamonds of the São Luiz deposit (*Brazil*). Russian Geology and Geophysics, 56, 296-305.
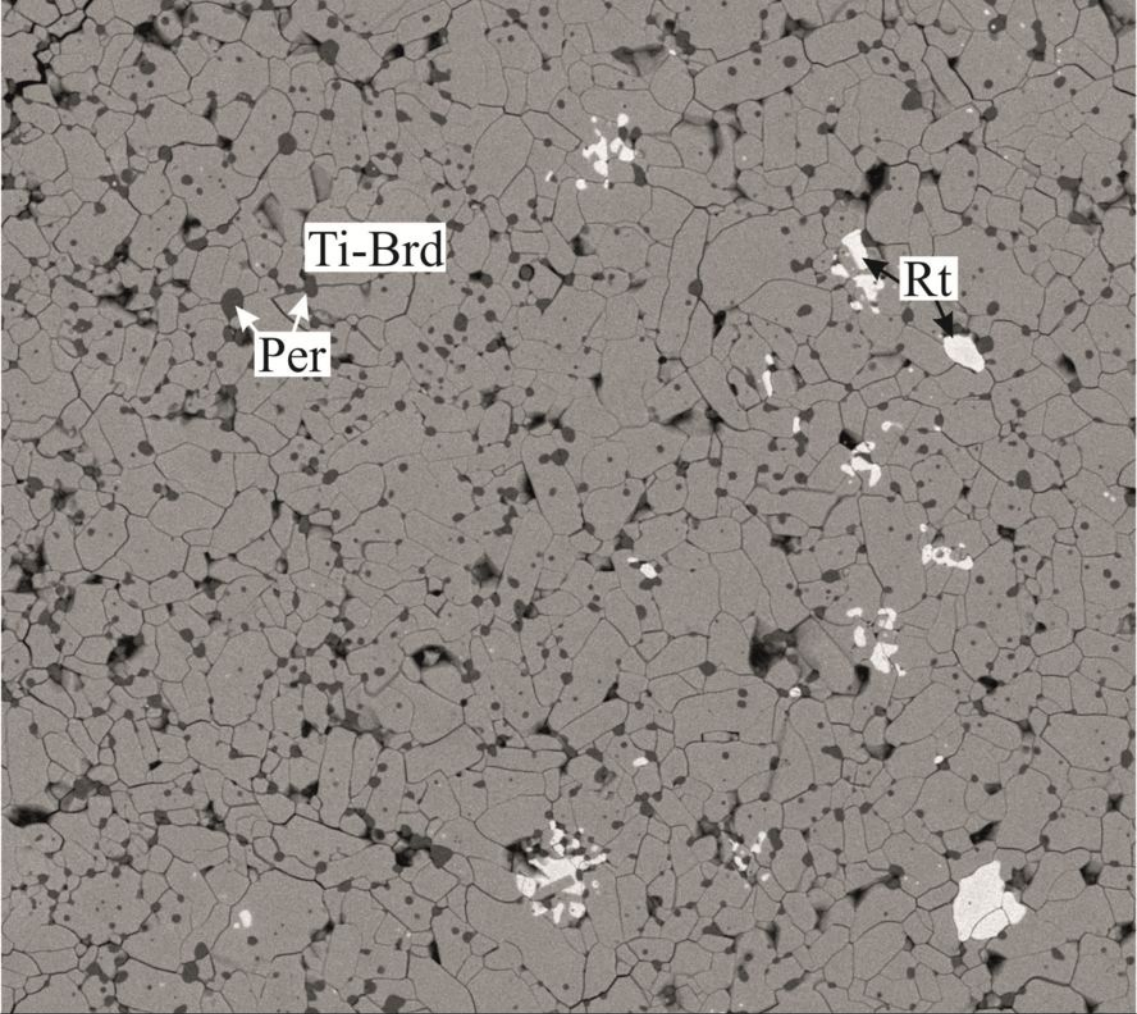
FIGURE CAPTIONS

FIGURE 1. SEM-BSE image of idiomorphic Ti-bearing bridgmanite-like (Ti-Brd) crystals associated with rutile (Rt) and periclase (Per) in the run 1608-70 [P = 20 GPa, T = 1600 °C]. CamScan electronic microscope MV2300.

FIGURE 2. The structure of the Ti-bridgmanite-like phase down [010]. Mg sites are given as spheres (red: MgA and MgB; yellow: MgC). Octahedra refers to the Ti site (dark blue) and to the (Si,Al) site (light blue). The unit-cell and the orientation of the structure are outlined.

FIGURE 3. Variation in tilting angle Φ of different bridgmanites with cation composition (Fe+Al) in cations per formula unit. Solid squares $MgSiO_3$ and $(Mg,Fe)SiO_3$, black open circles $(Mg,Fe)(Si,Al)O_3$, black open triangles $(Mg,Al)(Si,Al)O_3$, black down triangles $(Mg, Fe)SiO_3$ with 100 % $Fe^{3+}/\Sigma Fe$. Filled and empty red circles refer to the Ti-bridgmanite-like phase. Φ was calculated from the unit-cell parameters of literature data as follows: Ito and Yamada (1982), Kudoh et al. (1990), Parise et al. (1990), Mao et al. (1991), McCammon et al. (1992), Wang et al. (1994), Fei et al. (1996), Fiquet et al. (1998), Jephcoat et al. (1999), Bolfan-Casanova (2000), Andrault et al. (2001), Dobson and Jacobsen (2004), Walter et al. (2004), Nishio-Hamane et al. (2005, 2008), Vanpeteghem et al. (2006), Saikia et al. (2009), Tange et al. (2009), Catalli et al. (2011), Boffa Ballaran et al. (2012), Hummer and Fei (2012) and Sinmyo et al. (2014).

TABLE 1. Geometric details of Ti-bridgmanite.

MgA-polyhedron		*Ti-octahedron*	
MgA-O1	1.891(2)	Ti-O2 (×2)	1.8438(5)
MgA-O2	1.969(1)	Ti-O5 (×2)	1.9195(9)
MgA-O5 (×2)	2.200(1)	Ti-O4 (×2)	2.0094(9)
MgA-O5 (×2)	2.267(1)	average	1.924
MgA-O4 (×2)	2.477(1)	V_{Ti}	9.36
average	2.219	σ^2_{Ti}	29.13
		λ_{Ti}	1.0112
MgB-polyhedron			
MgB-O2	1.984(2)	*Si-octahedron*	
MgB-O3	2.064(1)	Si-O5	1.701(1)
MgB-O6 (×2)	2.169(1)	Si-O6	1.7148(9)
MgB-O4 (×2)	2.298(1)	Si-O6	1.7413(8)
MgB-O5 (×2)	2.395(1)	Si-O4	1.7614(8)
average	2.222	Si-O1	1.8187(5)
		Si-O3	1.8596(5)
MgC-polyhedron		average	1.766
MgC-O4 (×2)	1.897(1)	V_{Si}	7.20
MgC-O3	1.923(2)	σ^2_{Si}	40.97
MgC-O1	2.106(1)	λ_{Si}	1.0136
MgC-O6 (×2)	2.2559(9)		
MgC-O6 (×2)	2.4404(9)		
average	2.152		

Run 1608-70; P=20 GPa; T=1600°C   100 μm